# applied optics

# Harnessing diffraction grating in an in-plane switching cell submitted to zigzag lattice

Vincent Odent,[1,2,*] Ernesto Berrios-Caro,[1] and Marcel G. Clerc[1]

[1]*Departamento de Física, Facultad de Ciencias Físicas y Matemáticas, Universidad de Chile, Casilla 487-3, Santiago, Chile*
[2]*Université Lille 1, Laboratoire de Physique des Lasers, Atomes et Molécules, CNRS UMR8523 59655 Villeneuve d'Ascq Cedex, France*
*Corresponding author: vincent.odent@phlam.univ-lille1.fr*

Programmable diffraction gratings are relevant in optical data processing. One of the adequate device candidates is the in-plane switching liquid crystal cell. This technology, developed initially for liquid crystal screens, has also been studied with two inter-digital electrodes as a diffraction grating. Recently, the apparition of programmable zigzag wall lattices in an in-plane switching configuration has been reported. Here, we report a theoretical and experimental study of programmable diffraction grating in an in-plane switching cell.    © 2016 Optical Society of America

*OCIS codes:* (230.1950) Diffraction gratings; (230.3720) Liquid-crystal devices; (260.1960) Diffraction theory.

http://dx.doi.org/10.1364/AO.55.007803

## 1. INTRODUCTION

In-plane-switching (IPS) technology was developed initially for liquid crystal displays (LCD) to solve the twisted nematic (TN) field limitations. Since its introduction in 1996 [1,2], this technology has allowed for the improvement of screen qualities, especially color contrast and vision angles [3]. Moreover, IPS technology was also used as inter-digital electrodes, combined with liquid crystals, for switchable optical diffraction. A lot of liquid crystal phase grating designs have been reported that use this electrode configuration [4–7]. Their applications range from optical data processing and beam steering [8] to optical communication networking devices [9], which emphasize the relevance to controlling and understanding the different mechanisms existing in this kind of diffraction grating. Some works have studied the high voltage impact on the diffracted grating [10] or tested a new configuration with carbon nanotubes [11]. Latterly, the apparition of zigzag lattice in an IPS cell filled with nematic liquid crystal beyond a certain voltage threshold has been reported [12]. Recently, we have studied in detail, theoretically and experimentally, the zigzag instability of a wall lattice in a nematic liquid crystal with an IPS configuration [13]. We have also evidenced the importance of the liquid crystal molecule anchoring on their own dynamics when they are submitted to an external electrical forcing [14,15].

The aim of this paper is to investigate the zigzag wall lattice influence on the diffraction grating. We study an IPS cell used without liquid crystal. We confirm the diffractive nature of the empty cell, which works as diffraction grating with a low contrast. This property changes when we consider this cell filled with a nematic liquid crystal subjected to a given voltage.

We propose an analytical model to reproduce a zigzag lattice, which gives us the typical $x$ signature of the diffraction image. Numerical simulations of a more realistic/imperfect zigzag lattice, taking into account the different experimental properties, show quite good agreement with the experimental observations. This method allows us make evident a dispersion of the amplitude and the wavelength of the zigzag lattice inside the sample.

## 2. EXPERIMENTAL SETUP

The experimental setup is depicted in Fig. 1. We use two identical cells, one empty (without liquid) and the second one filled with a nematic liquid crystal. We consider IPS cells with a homogeneous planar alignment [following the $x$-axis, cf. Fig. 1(a)] and a parallel rubbing to the electric field (Instec, IPS02A89uX90). The indium tin oxide (ITO) electrode width and the gap width are the same; $\epsilon = 15$ μm. The height of the electrodes is negligible ($\sim$25 nm) compared to the cell thickness ($d = 8.9 \pm 0.2$ μm). The active zone is a square of side $l = 1$ cm. Under these settings, we can consider the cell in a good approximation as an infinite media. The liquid crystal cell is composed of a layer of $E7$ nematic liquid crystal, which is inserted between two glass plates (thickness $g = 1.1$ mm). The elastic constants of the liquid crystal are, respectively, $K_1 = 11.2$, $K_2 = 6.8$, and $K_3 = 18.6(\times 10^{-12}$ N). The parallel and the perpendicular dielectric constants are $\varepsilon_\parallel = 18.96$ and $\varepsilon_\perp = 5.16$ [16,17]. The cell electrodes are connected to a function generator. The typical parameter range for the frequency is $\sim$200 mHz – 2 MHz and for the amplitude $\sim$10 $V_{PP}$ – 20 $V_{PP}$ (volt peak-to-peak). We illuminate
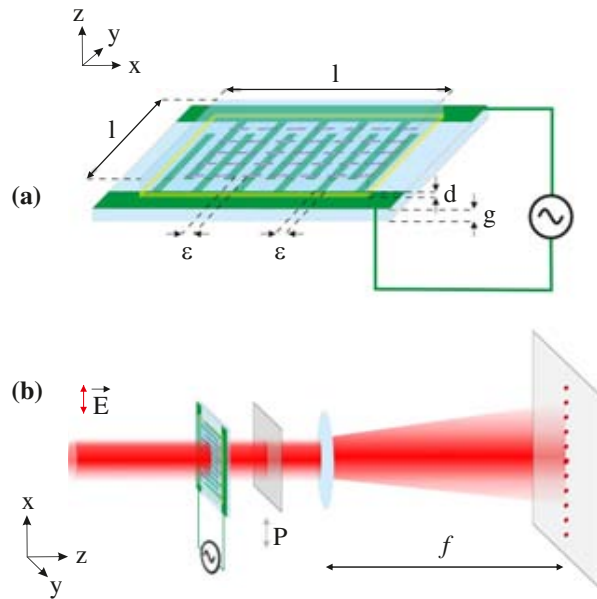
**Fig. 1.** (a) Schematic representation of the liquid crystal IPS cell, connected to a generator. Thickness between the two glass plates, $d = 8.8 \pm 0.2$ μm. Thickness of a glass plate, $g = 1$ mm. Active zone, $l \times l = 1$ cm$^2$. Gap between two electrodes, $\epsilon = 15$ μm. (b) Sketch of the experimental setup: $\vec{E}$, vertically polarized collimated beam; $P$, vertical linear polarizer; $f$, focal distance of the imaging lens.

the cell with a vertically polarized helium–neon laser beam at 632.8 nm, as shown in Fig. 1(b). The beam is previously collimated, using a telescope, in order to consider the Fraunhofer approximation valid. The beam waist is $w = 1.1$ mm. The laser power is sufficiently weak to prevent the molecular reorientation, which is typically $P_0 = 1$ mW. A linear polarizer is placed behind the cell. We generate, on a screen, the diffraction figure placed in the focal plane of a convergent lens. We record the diffusive light of the diffraction figure on the screen with a CCD monochrome camera. By replacing the screen by a power meter, we have the possibility of recording the power value of every diffracted order until the sixth one.

## 3. DIFFRACTION THEORY WITH AN EMPTY CELL

In the literature, there are several reports about liquid crystal phase grating based on IPS [9,10,18]. However, to the best of our knowledge, no works study the transmission of the empty cell. We propose a simple diffraction grating model, which evidences the ITO electrodes as a diffraction grating.

### A. One-dimensional Frauhofer Diffraction Theory

We consider the most simple model to reproduce the Fraunhofer diffraction phenomenon with an empty IPS cell. The cell is constituted by two parallel glass layers and two electrode combs of ITO, which are stuck on one glass layer (inside the cell), as represented in Fig. 2(a).

One can calculate the diffraction figure from the intensity transmission function $t(x)$ (diffraction grating) [19,20]. This one is a crenel function, following the $x$ axis, as represented
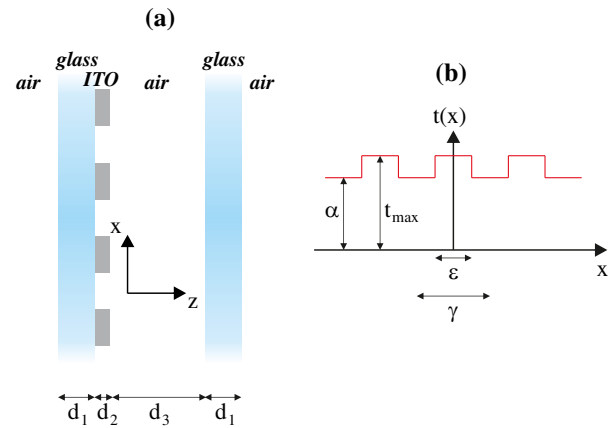


**Fig. 2.** (a) Sketch of an empty IPS cell that is constituted by two parallel glass layers and two electrode combs of ITO, and (b) the cell intensity transmission function.

in Fig. 2(b). To simplify, we evaluate $t_{\max} = 1$, which is the light part that crosses only the two glass layers, and we consider $\alpha$ as the transmission coefficient in amplitude of the light which crosses the glass layers and the electrodes. $\epsilon$ is the electrode width, and $\gamma$ is the distance between two electrodes. Hence,

$$t(x) = \begin{cases} 1, & -\frac{\epsilon}{2} + n\gamma < x < \frac{\epsilon}{2} + n\gamma \\ 1 - \alpha & \frac{\epsilon}{2} + n\gamma < x < \frac{3\epsilon}{2} + n\gamma. \end{cases} \quad (1)$$

The diffraction figure is given by

$$I(u) = |E|^2 = \left| \int_{-\gamma/2}^{\gamma/2} \sum_{n=0}^{N} t(x - x_n) e^{-2\pi i u x} dx \right|^2, \quad (2)$$

where $N$ is the electrode numbers illuminated by the light source, $t(x)$ is the amplitude transmission function, and $2\pi u$ is the wavenumber. After the straightforward calculations from Eq. (2), we obtain the diffraction figure in the Fourier space.

$$I(u) = \frac{\sin^2(\pi u \gamma N)}{\sin^2(\pi u \gamma)} [\alpha \gamma \sin c(\pi u \gamma) + (1 - \alpha)\epsilon \sin c(\pi u \epsilon)]^2. \quad (3)$$

Considering the experimental electrode sizes, we have $\gamma = 2\epsilon$. We calculate the zero diffraction order from the equation above:

$$I(0) = N^2 \epsilon^2 [1 + \alpha]^2. \quad (4)$$

The other diffraction orders are given by

$$I(2m/\gamma) = 0, \quad (5)$$

and

$$I((2m + 1)/\gamma) = \frac{4N^2 \epsilon^2}{\pi^2 (2m + 1)^2} [1 - \alpha]^2, \quad (6)$$

where $m$ is an integer number.

The experimental procedure to determine the coefficient $\alpha$ is done by measuring the different diffraction orders. Indeed, the theoretical $\alpha$ determination can be distorted by other phenomena, such as glass layer interferences, anchoring treatment, inhomogeneities, and imperfection, among others.

## B. Experimental Transmission Coefficient Determination

The $\alpha$ value is determined experimentally by evaluating the diffraction order ratio. We consider the six first diffraction orders. The experimental values are reported in Table 1.

From Eqs. (4) and (6), we calculate the three following diffraction order ratios:

$$\frac{I(0)}{I(1/\gamma)_{\text{theo}}} = \frac{\pi^2}{4}\left[\frac{1+\alpha}{1-\alpha}\right]^2, \tag{7}$$

$$\frac{I(1/\gamma)}{I(3/\gamma)_{\text{theo}}} = 9, \tag{8}$$

$$\frac{I(1/\gamma)}{I(5/\gamma)_{\text{theo}}} = 25. \tag{9}$$

Note that the odd diffraction orders do not depend on the $\alpha$ value. The theoretical ratios from Eqs. (8) and (9) present a good agreement with their experimental observations:

$$\frac{I(1/\gamma)}{I(3/\gamma)_{\text{exp}}} = 9.9, \tag{10}$$

$$\frac{I(1/\gamma)}{I(5/\gamma)_{\text{exp}}} = 23.6. \tag{11}$$

By rewriting Eq. (7), we find

$$\alpha = \frac{2\sqrt{\frac{I(0)}{I(1/\gamma)}} - \pi}{2\sqrt{\frac{I(0)}{I(1/\gamma)}} + \pi}. \tag{12}$$

The experimental ratio $I(0)/I(1/\gamma)$ gives us $\alpha = 0.70$. Hence, the empty cell plays the role of a diffraction grating, however, with a lower efficiency (low contrast). Indeed, the visibility, for the empty cell is $V = 0.09$.

## 4. DIFFRACTION THEORY WITH A LIQUID CRYSTAL CELL

A lot of studies have evaluated the diffraction efficiency of the one-dimensional (1D) spot pattern [9,18,21,22]. In particular, Han has presented the diffraction efficiency, with a sample where the zigzag instability exists [12]. We complete this characterization by adding a frequency study. Figure 3 shows the diffraction efficiency of our sample depending on the voltage amplitude, between $T = 0$ $V_{pp}$ and $T = 100$ $V_{pp}$, and the

**Table 1. Experimental Intensity of the First Diffraction Orders of an Empty In-plane Switching Cell**

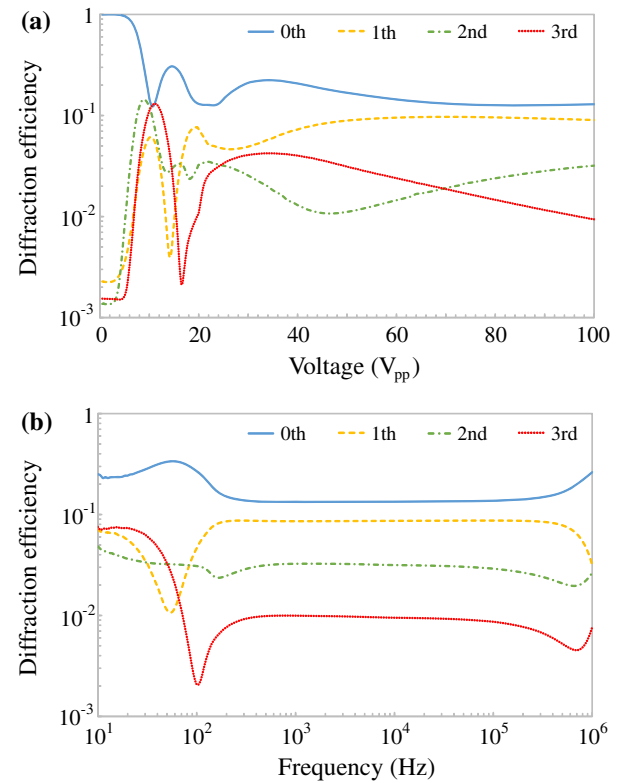| Diffraction Order | Power Values ($\mu$W) |
|---|---|
| 0 | 576 |
| 1 | 31.8 |
| 2 | 1.1 |
| 3 | 3.20 |
| 4 | 0.89 |
| 5 | 1.36 |



**Fig. 3.** Diffraction efficiencies of the zeroth to fourth order. (a) Voltage evolution for $f = 1$ kHz, and (b) frequency evolution for $T = 20$ $V_{pp}$.

frequency, between $f = 10$ Hz and $f = 1$ MHz. The diffraction efficiency is defined as

$$D_e = I/I_0, \tag{13}$$

where $I$ is the order of diffracted intensity, and $I_0$ is the total transmitted light. Figure 3(a) qualitatively gives the same results as the Han evaluation, given that the liquid crystal mixture is the same, $E7$, and the liquid crystal cells have a small difference around the electrode gaps. We observe in Fig. 3(a) a strong diffraction order modification between $T = 8$ $V_{pp}$ and $T = 30$ $V_{pp}$ for a fix frequency value of $f = 1$ kHz. For a fixed tension amplitude value $T = 20$ $V_{pp}$, we also observe, in Fig. 3(b), a strong modification of the diffraction orders between $f = 10$ Hz and $f = 1$ kHz. This information helps us evaluate the region of parameters, where the liquid crystal dynamics change a lot and, consequently, its diffraction figure.

Recently, we have observed that below a voltage threshold (amplitude or frequency), the cell filled with a liquid crystal exhibits an Ising wall lattice which becomes a zigzag instability [13]. To confirm these phenomena, we have used parallel polarizers and observe black bands (Ising wall lattice) and black zigzags (zigzag instability). We use this configuration to generate a programmable diffraction grating.

## A. Perfect Zigzag Lattice: Two-dimensional Fraunhofer Diffraction Theory

In a first approximation, we assume to have a perfect two-dimensional (2D) diffraction mask, with a periodic black zigzag, as represented in Fig. 4(a). The zigzag pattern presents a constant amplitude and a constant wavelength. The lattice does not present a phase shift between the different zigzag instabilities. In this ideal case, we assume to have a visibility of $V = 1$, so $\alpha = 0$. $\theta$ is the angle between the $y$ axis and the zigzag lines. The diffraction mask, represented in Fig. 4(a), gives the following diffraction figure in the Fourier space:

$$I(u,v)$$
$$= \left| \int_{-b/2}^{b/2} \int_{-a/2-y\tan\alpha}^{a/2-y\tan\alpha} \sum_{n=0}^{N} \sum_{m=0}^{M} t(x-x_n, y-y_m) e^{-2\pi i(ux+vy)} \,dx\,dy \right|^2. \quad (14)$$



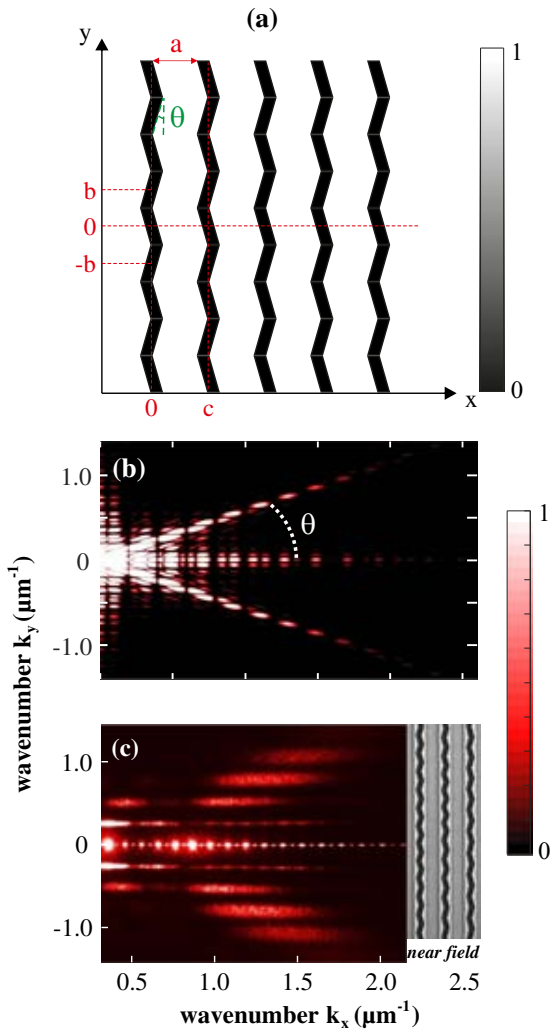**(a)**



**(b)**



**(c)**

**Fig. 4.** (a) 2D perfect diffraction zigzag grating. (b) Diffraction image obtained from a 2D perfect diffraction zigzag grating using Eq. (15). (c) Experimental diffraction image obtained from an IPS cell with a zigzag lattice. Inset accounts for a snapshot of the cell, $f = 100$ Hz, and $T = 20$ $V_{pp}$.

After straightforward calculations, we obtain

$$I(u,v) = \frac{\sin(\pi u c N)}{\sin(\pi u c)} \frac{\sin(2\pi v b M)}{\sin(2\pi v b)} ab \sin c(\pi u a).$$
$$[\sin c(\pi b(v - u \tan(\theta))) + \sin c(\pi b(v + u \tan(\theta)))], \quad (15)$$

where $c$ is the period of the grating following the $x$ axis. Its value is imposed by the distance between two electrodes in the cell ($c = \gamma$, cf. Fig. 2). $a$ is the thickness of the white bands. We have the condition $a > \epsilon$. Physically, $a$ represents the distance where liquid crystal molecules are not subjected to electro-reorientation [13]. $2b$ is the period of the zigzag instability. $\theta$ is the zigzag angle. $N$ is the number of electrodes illuminated by the light, and $cN$ is the transverse size of the illuminated cell following the $x$ axis. $M$ is the number of zigzags illuminated by the light, and $bM$ is the transverse size of the illuminated cell following the $y$ axis. With a Gaussian beam, we have the following equality: $bM = cN$.

The diffraction figure, obtained from Eq. (15), is depicted in Fig. 4(b). Notice the presence of two lines at $\theta$ degrees in the Fourier plane. Indeed, these two lines are a signature of the zigzag lattice.

However, the diffraction figure does not correspond exactly to the experimental diffraction figure, presented in Fig. 4(c). Indeed, the near field of the zigzag lattice presents some irregularities that are not taken into account in this perfect zigzag lattice. We will now consider a more realistic zigzag lattice.

## B. Imperfect/Real Zigzag Lattice: 2D Fast Fourier Transform

To have an adequate description of the experimental findings, we consider an imperfect zigzag grating. We present a portion of the zigzag grating in Fig. 5, used as near field. The matrix used contains $8192 \times 8192$ pixels with a spatial resolution of $\Delta x = \Delta y = 0.1$ μm and a distance between two electrodes that is $\gamma = 30$ μm. The wavelength, $\lambda(x,y)$, and the thickness, $D(x,y)$, of the black zigzag lattice have a small variation depending on the location in the cell. We define for every
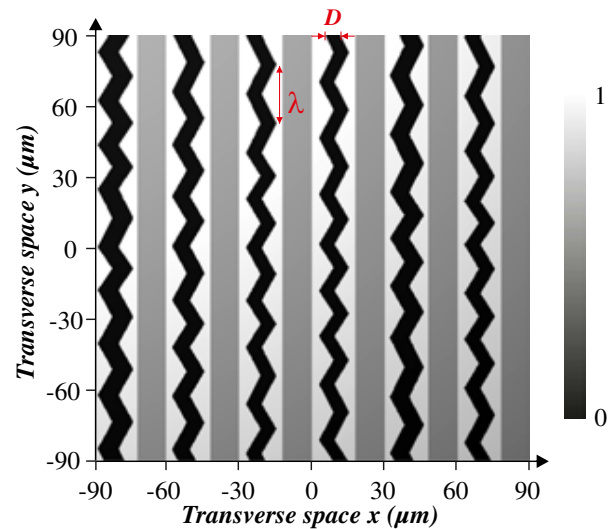


**Fig. 5.** Portion of the imperfect zigzag grating. $\lambda_0$ is the average wavelength, and $D$ is the black zigzag average thickness.

period a wavelength $\lambda(x, y) = \lambda_0 \pm \delta\lambda(x, y)$, where $\delta\lambda(x, y) = \lambda_0\eta(x, y)/B_1$, and $\eta(x, y)$ is a random function giving a value between zero and one with a uniform distribution. In the same way, we define the thickness $D(x, y) = d \pm \delta d(x, y)$, where $\delta d(x, y) = d\eta(x, y)/B_2$. The observation on the experimental pictures of the sample by a microscope provides a more complex intensity profile than the crenel function, as presented in Fig. 2(b). Consequently, we had another grating on the zigzag grating. The cell is illuminated by a delimited laser source. We also take into account this effect in Fig. 5.

We calculate the diffraction image by using the 2D fast Fourier transform. We evaluate the parameters $B_1$ and $B_2$ by a quantitative comparison between the experimental (top) and numerical diffraction (bottom) figure presented in Fig. 6. Notice that we have chosen these parameters to obtain numerically diffractive images similar to those observed experimentally. Hence, experimental diffractive images can be reproduced qualitatively by the use of a simple model.

## 5. EXPERIMENTAL RESULTS

### A. Low Frequency: $f = 10$ Hz

At $f = 10$ Hz and with a voltage tension of $T = 20$ V$_{pp}$, the liquid crystal cell exhibits a roll lattice in the near field, see the inset in Fig. 6(a), which corresponds to a snapshot of the cell. The experimental image in the Fourier space is a 1D pattern with a wavenumber of $k_{10\,Hz} = 0.104$ µm$^{-1}$. This wavenumber corresponds to a diffraction image with a diffraction step of $\lambda_{10\,Hz} = 60.4$ µm. We explain the factor of 2 difference ($\lambda_{10\,Hz} = 2\gamma$, where $\gamma$ is the diffraction grating step) by the fact

that at this low frequency the black bands appear and disappear successively on the first electron comb and then on the second one. However, this temporal oscillation is not recorded on the near field image, which corresponds to a temporal average of the roll lattice dynamics. Considering this effect, the diffraction grating step is exactly $2\gamma$, then we have a quite good agreement between the experimental and the numerical far field figure in Figs. 6(a) and 6(d).

### B. Middle Frequency: $f = 100$ Hz

At $f = 100$ Hz with a voltage tension $T = 20$ V$_{pp}$, the system presents a zigzag lattice. The zigzag signature in the Fourier space is the X structure with an angle $\pm\theta$. We note the presence of different bands. The band's thickness is directly linked to the $\lambda$ dispersion. In this case, we evaluate $B_1 = 5$. The dispersion of $D$ erases the vertical black lines due to destructive interferences. We evaluate $B_2 \simeq 7$. By taking into account these two dispersion parameters, we have a fairly good agreement between the experimental and the numerical diffraction figures, represented in Figs. 6(b) and 6(e).

### C. High Frequency: $f = 1.3$ MHz

At $f = 1.3$ MHz with a voltage tension $T = 20$ V$_{pp}$, we observe a sinusoidal lattice. We detect in the Fourier space two opposite (following $k_y = 0$) and intense lines. They represent the fundamental frequency of the sinusoidal functions. Some harmonics can also be seen. To confirm this observation, we modify the theoretical lattice with sinusoidal functions, and we evaluate $B_1 = 5$ and $B_2 \simeq 14$. We qualitatively obtain the same diffraction image.
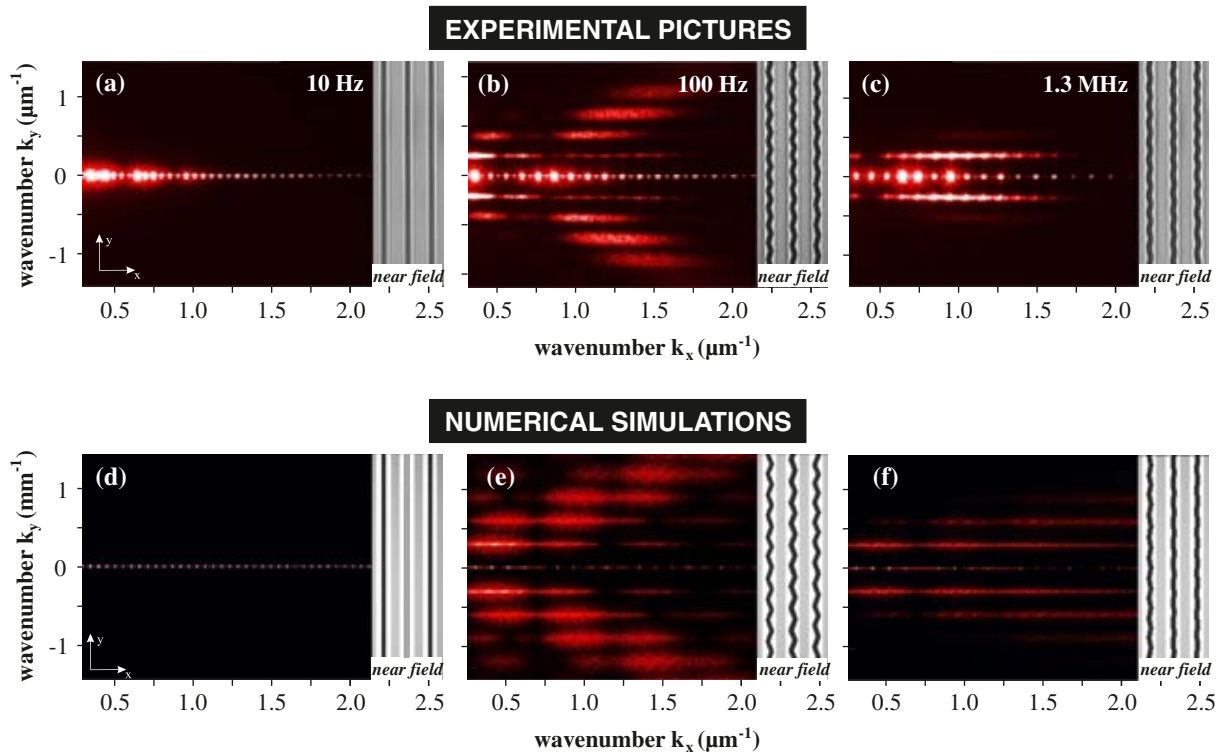


**Fig. 6.**   Diffractive and near field images observed for different frequencies, (a) $f = 10$ Hz, (b) $f = 1.3$ MHz, and (c) $f = 10$ Hz, with a voltage of 20 V$_{pp}$. The top and bottom panels correspond to experimental and numerical observations, respectively.
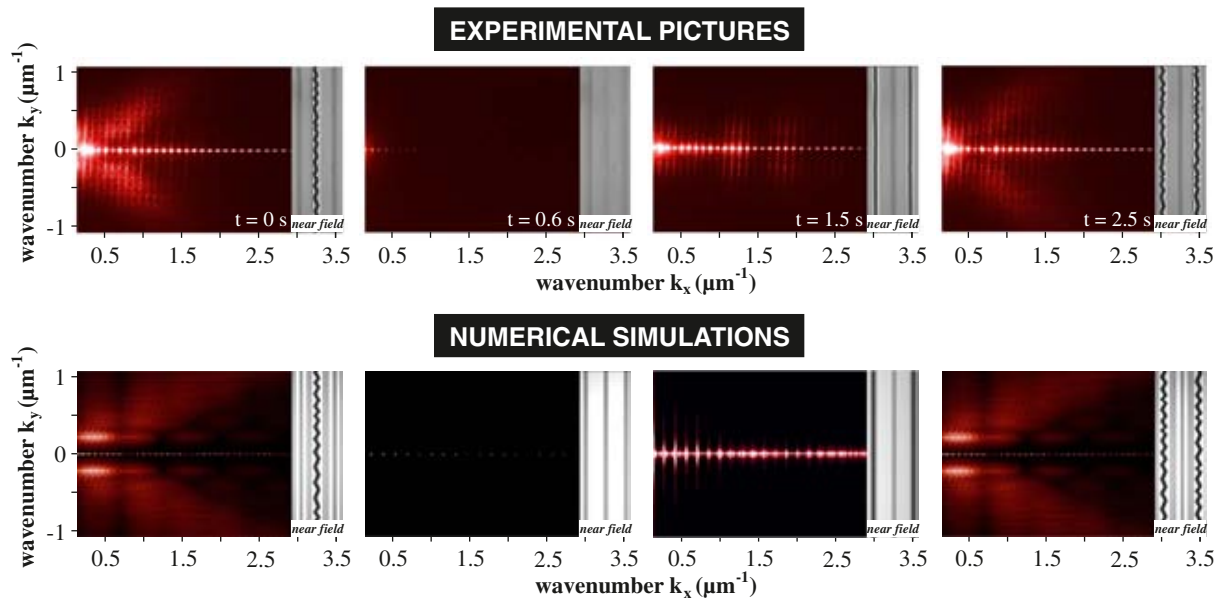
**EXPERIMENTAL PICTURES**



**NUMERICAL SIMULATIONS**



**Fig. 7.**    Temporal sequence of diffractive figures observed for a semi temporal period with $f = 200$ mHz, and $T = 20$ V$_{pp}$. The top and bottom panels correspond to the experimental and numerical observations, respectively.

## D. Very Low Frequency: $f = 200$ mHz

At a very low frequency of $f = 200$ mHz with the same voltage, the system cannot be considered stationary. The liquid crystal exhibits a conductive regime. The liquid crystal space charges oscillate with the electrical field. This phenomenon can be attributed to the gradient flexoelectric effects [23]. It has temporal dynamics directly linked to the voltage frequency. Figure 7 shows four pictures during the half period of the sinusoidal voltage. At $t = 0$ s, the central electrode in the near field presents a zigzag instability with a not well defined wavelength. Consequently, the diffraction image presents a X with large arms. We evaluate for our model $B_1 = 0.5$ and $B_2 \simeq 7$, which has a good agreement with the experimental observations.

## E. Application

We have highlighted the results of programmable lattice that shows that one can generate more complex diffraction figures than those presented in the literature. First, these diffraction images give us some information about the molecular reorientation inside the cell, as well as the dispersion of the wavelength and the amplitude of the zigzag lattice. Second, the formation of a 2D diffraction image extends the possibility of beam steering and optical communication networking devices and the characterization of atomic spectra. Finally, this type of diffraction may allow for information about spatial structures of complex light sources.

## 6. CONCLUSION

Programmable diffraction gratings open the possibility of new optical data processing, characterization of atomic spectra with applications in astronomical observations, space flight instruments, and synchrotron spectrometers, among others. In this work, we have established the possibility of creating this kind of programmable grating. We have characterized an empty IPS cell and seen that it is like a bad diffraction grating. In contrast, an IPS cell filled with a nematic liquid crystal subjected to a given voltage exhibits a rich complex diffraction pattern. Applying a small voltage into a wide range of frequencies, the sample exhibits a stripe diffraction grating. Increasing the voltage, this diffractive pattern presents a spatial instability generating an undulating diffraction grating, and at higher voltages it becomes a zigzag type. We have analytically given a first approximation of the diffraction image obtained with a perfect zigzag lattice. Then, we have studied, experimentally and numerically, the diffractive image and observed a complex structure in the perpendicular direction to the "traditional 1D pattern" in the diffraction image. We have evidenced with this structure a variation/dispersion of the amplitude and the wavelength of the zigzag instability.

One of the limitations of our programmable diffraction gratings is that the time response of liquid crystals is slow on the order of milliseconds. However, this allows us to establish the proof of concept of manipulable diffraction grating. The possibility of faster programmable diffraction gratings using soft or solid materials is a still open question.

## REFERENCES

1. M. Oh-e and K. Kondo, "Electro-optical characteristics and switching behavior of the in-plane switching mode," Appl. Phys. Lett. **67**, 3895–3897 (1995).
2. M. Oh-e, M. Ohta, S. Aratani, and K. Kondo, "Principles and characteristics of electro-optical behavior with in-plane switching mode," in *Proceedings of 15th International Display Research Conference* (Society for Information Display, 1995), pp. 577–580.
3. Y. Sun, Z. Zhang, H. Ma, X. Zhu, and S.-T. Wu, "Reflective in-plane switching liquid crystal displays," J. Appl. Phys. **93**, 3920–3925 (2003).
4. J. Chen, P. J. Bos, H. Vithana, and D. L. Johnson, "An electro-optically controlled liquid crystal diffraction grating," Appl. Phys. Lett. **67**, 2588–2590 (1995).
5. H. Murai, "Electro-optic properties of liquid crystal phase gratings and their simulation using a homogeneous alignment model," Liq. Cryst. **15**, 627–642 (1993).
6. R. Ramsey and S. C. Sharma, "Switchable holographic gratings formed in polymer-dispersed liquid-crystal cells by use of a He–Ne laser," Opt. Lett. **30**, 592–594 (2005).
7. C. W. Christenson, C. Greenlee, B. Lynn, J. Thomas, P. Blanche, R. Voorakaranam, P. S. Hilaire, L. J. Lacomb, R. A. Norwood, M. Yamamoto, and N. Peyghambarian, "Interdigitated coplanar electrodes for enhanced sensitivity in a photorefractive polymer," Opt. Lett. **36**, 3377–3379 (2011).
8. T. Scharf, M. Bouvier, and R. Dandliker, "Multilevel nematic liquid crystal phase grating," Proc. SPIE **4418**, 31–37 (2001).
9. I. Fujieda, O. Mikami, and A. Ozawa, "Active optical interconnect based on liquid-crystal grating," Appl. Opt. **42**, 1520–1525 (2003).
10. J.-W. Han, "Optical diffraction effects of grating cells fabricated using polymer-dispersed liquid crystals," Mol. Cryst. Liq. Cryst. **534**, 69–80 (2011).
11. K. Won, A. Palani, H. Butt, P. J. W. Hands, R. Rajeskharan, Q. Dai, A. A. Khan, G. J. Amaratunga, H. J. Coles, and T. D. Wilkinson, "Electrically switchable diffraction grating using a hybrid liquid crystal and carbon nanotube-based nanophotonic device," Adv. Opt. Mater. **1**, 368–373 (2013).
12. J. Han, "Comparison of optical diffraction gratings fabricated using in-plane switching cells," J. Korean Phys. Soc. **60**, 1361–1366 (2012).
13. I. Andrade-Silva, M. G. Clerc, and V. Odent, "Zig-zag wall lattice in a nematic liquid crystal with an in-plane switching configuration," Phys. Rev. E **90**, 022504 (2014).
14. I. Andrade-Silva, M. G. Clerc, and V. Odent, "Asymmetric counterpropagating fronts without flow," Phys. Rev. E **91**, 060501 (2015).
15. I. Andrade-Silva, M. G. Clerc, and V. Odent, "Asymmetric counter propagation of domain walls," Commun. Nonlinear Sci. Numer. Simul. **36**, 192–203 (2016).
16. P. Oswald and P. Pieranski, *Nematic and Cholesteric Liquid Crystals* (Taylor & Francis, 2005).
17. I. C. Khoo, *Liquid Crystals*, 2nd ed. (Wiley, 2007).
18. I. Fujieda, "Liquid-crystal phase grating based on in-plane switching," Appl. Opt. **40**, 6252–6259 (2001).
19. D. Rittenhouse, "An optical problem, proposed by Mr. Hopkinson, and solved by Mr. Rittenhouse," Trans. Am. Philos. Soc. **2**, 201–206 (1786).
20. J. Fraunhofer, "Neue Modifikation des Lichtes durch gegenseitige Einwirkung und Beugung der Strahlen, und Gesetze derselben," Denkschriften der Königlichen Akademie der Wissenschaften zu München **8**, 3–76 (1821).
21. C. Desimpel, H. Neyts, I. Janevska, A. Gjurcinovski, D. K. G. De Boer, and R. Cortie, "Polarization state of the diffraction peaks in in-plane switching cells," in *Proceedings of the 21st International Display Research Conference in Conjunction with the 8th International Display Workshops* (2001), pp. 161–164.
22. I. Drevensek-Olenik, M. Copic, M. E. Sousa, S. P. Gorkhali, and G. P. Crawford, "Optical diffraction properties of polymer dispersed liquid crystals switched by interdigitated electrodes," Mol. Cryst. Liq. Cryst. **438**, 251–261 (2005).
23. K. S. Krishnamurthy and P. Kumar, "Emergence of periodic order in electric-field-driven planar nematic liquid crystals: an exclusive ac effect absent in static fields," Phys. Rev. E **76**, 0517051 (2007).